Laser damage thresholds of underwater anti-reflection coatings for face-cooling of high power Yb:YAG laser disks

Jérôme Lhermite, L. Lamaignère, Z. Cole, D. Descamps, G. Duchateau, Ch. Féral, D. Marion, E. Mével, M.-Ch. Nadeau, Sylvain Petit, et al.

Laser damage thresholds of underwater anti-reflection coatings for face-cooling of high power Yb:YAG laser disks

J. Lhermite[a], L. Lamaignère[b], Ph. Balcou[a,*], Z. Cole[c], D. Descamps[a], G. Duchateau[b], Ch. Féral[a], D. Marion[a], E. Mevel[a], M.-Ch. Nadeau[a], S. Petit[a], A. Rohm[a], G. Rouzaud[b]

[a] *Univ. Bordeaux, CEA, CNRS ; CELIA (Centre Lasers Intenses et Applications), UMR 5107, Talence, F-33400, France*
[b] *CEA, CESTA, Le Barp, F-33116, France*
[c] *Teledyne FLIR, Bozeman, MT 59715, USA*

Abstract

Achieving high laser damage thresholds of face-cooled amplifier slabs is an important issue to develop high average power lasers. We report an investigation of the Laser Induced Damage Threshold (LIDT) of Ion Beam Sputtering (IBS) hafnium oxide anti-reflection layers deposited on Yb:YAG crystals, designed to be embedded in a flowing water coolant while submitted to 1 μm laser irradiation, and compare the damage thresholds in air and underwater. The measured damage thresholds turn out to be consistent with the best values obtained on similar coatings, and are at least equal, or even higher, underwater than in air. An electromagnetic model is presented based on water permeation into the coating, that displays stronger field enhancements in air than underwater next to the sub-surface damage precursors, offering a possible explanation. Our results validate the possibility to use anti-reflection coatings for Yb:YAG crystals face-cooled in water, at fluences equal to or higher than the saturation fluence of Yb:YAG at room temperature.

Keywords: Laser Induced Damage Threshold, anti-reflection coating, Ytterbium-YAG, water face-cooling, high average power lasers

*philippe.balcou@u-bordeaux.fr

1. Introduction

The field of physics and technology of short pulse and ultra-high intensity lasers features two main technological frontiers: ultra-high peak powers on one hand, and high average powers on the other hand, bound to be instrumental to reach high profile applications such as high luminosity electron beams accelerators. The quest for ever higher average powers of intense lasers is therefore crucial; thermal issues within the laser amplifiers are known to be one essential key issue to solve, along with high-power diode pumping.

Among the techniques currenly used to optimize cooling of amplifying media, direct face cooling of high power amplifying slabs, directly immersed in a cooling flow, was proposed by Okada et al. [1], and Zuegel et al. [2] and has recently attracted worldwide attention, especially for systems where the laser beam size or energy exceed the capabilities of thin disk technologies [3].

Two main techniques exist for face-cooling: gas flow cooling, in which the gas is most frequently cryogenic helium, up to the kW landmark [4], at the expense of heavy cryo-cooling infrastructures; and liquid cooling [5], in which the coolant is most often water or deuterated water, or a family of fluorinert, or possibly special oils. This technology allowed impressive progress on the output power of laser resonators [6].

In both cryo-gas and liquid face-cooling, a further key issue is the damage threshold of the antireflection coatings of the amplifying laser slabs. Two important studies [4, 7] were reported recently on the damage threshold of slabs under He gas cooling, or of active mirrors, at cryogenic temperatures.

In a cryogenic helium gas-cooled multi-slab configuration, Divoký et al. [4] have pointed out that most commercial multilayers have a damage threshold at a fluence as low as 1.5 J/cm^2 in their experimental conditions (1 ns pulses, very low temperatures); these authors were able to increase this value up to 3 J/cm^2 after a careful screening and optimization of multilayer materials and technologies.

Higher Laser Induced Damage Thresholds (LIDT) values were reported by Wang et al. [7] for helium-cooled active mirrors; however it is difficult to compare directly numerical values of LIDTs, since these values have to be rescaled with respect to the temporal duration of the test bench laser, and may also depend on other factors, as the exact LIDT definition, or the focal spot size of the test laser.

In all cases, the essential issue is to improve the LIDT up to values allowing operation of the laser amplifier close to the saturation fluence of the

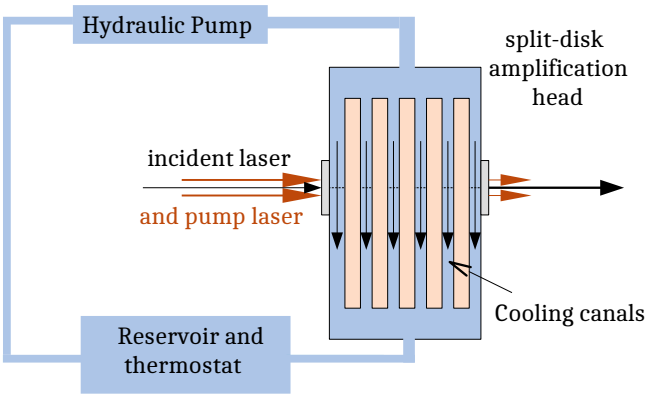

Figure 1: Principle of a liquid face-cooled split disk amplifier head, in which a liquid coolant is circulated and thermalized, then injected into cooling canals in between multiple amplifier disks.

amplifying crystal, which, for Yb:YAG, stands around 8 J/cm^2 at room temperature [8].

The HORIZON project aims to develop cutting-edge technologies for a kW-class, liquid face-cooled, terawatt chirped-pulse amplification (CPA) laser operating with Yb:YAG at 1030 nm [9, 10]. The amplifier face coolant was chosen to be either de-ionized water (conductivity < 3 mS), or deuterated water. In the HORIZON laser architecture, the chirped pulse duration during amplification is 1 ns, so that this duration should be the reference for all damage tests described below.

Figure 1 shows the principle of a typical liquid face-cooled amplifier head: the amplifier medium consists of series of slabs, located in a chamber with a continuous flow of coolant in between the slabs, and between the side slabs and the windows. In the HORIZON project, the series of slabs is an ensemble of three Yb:YAG disks supplied by Teledyne FLIR Laser Crystals. The disk widths are either 2.3 mm or 3.2 mm, longitudinally pumped at 940 nm in a continuous wave regime. The coolant is put in motion, thermalized and filtered by an external hydraulic system.

Such a configuration with permanent operation underwater raises questions on the capability of multilayer antireflection coatings deposited on the Ytterbium:YAG crystals, and permanently immersed under water, to withstand the laser flux. The physics of damage may indeed depend strongly

on the nature of the layers and of the ambiant medium. For example, [11] have studied LIDTs of hafnium oxide layers, similar to ours, in air; [12] have reported LIDTs under vacuum conditions, with a fatigue damage behavior depending on the remaining oxygen and water vapor densities; [13] have reported the effect of water vapor in air on the thermal conductivities of layers, and on the damage thresholds. However, the behavior of antireflection coatings directly under water has not been investigated so far to the best of our knowledge.

It is therefore crucial to test the anti-reflection coatings in the same environment that prevails in the amplifier head, i.e. immersed in water. The present article presents the results of series of laser-induced damage tests performed on two disks on the BLANCO laser damage testbed at the Centre d'Etudes Techniques d'Aquitaine, Commissariat à l'Energie Atomique et aux Energies Alternatives (CEA CESTA), Le Barp, France. We first detail the materials and methods used; we then present the experimental results for Laser-Induced Damage Thresholds, following standard procedures (1-on-1, rasterscan) [14]. We discuss the most salient experimental results, first ruling out thermal or optical non-linear issues, and suggest an interpretation in the frame of an electromagnetic model. We conclude on the perspectives opened by the strinkingly good results of LIDTs underwater.

2. Materials and damage threshold measurement method

2.1. Sample description

Two crystal samples were used for LIDT studies, identical and from the same boule and coating batch as the crystal in operation on the HORIZON prototype laser.

They are Ytterbium-doped Yttrium Aluminum Garnet disks, 70 mm in diameter; the first disk has a thickness of 3.2 mm and a doping of 2 atom$-\%$ (sample A); the second has a thickness of 2.3 mm and doping of 1.5 atom$-\%$ (sample B). Due to limited surface available on the disks, there was no attempt to reverse the orientation of the disks; moreover damage sites were observed essentially on the rear surfaces, showing that the physics of damage triggering is related to the rear surface and antireflection layer. To that respect, referring to samples A and B means the rear surfaces of the 3.2 mm and 2.3 mm disks, respectively.

The anti-reflection coatings, from Advanced Thin Films Inc., are designed to be operated under water; they consist of layers of HfO_2 and SiO_2. The

coating technology was Ion Beam Sputtering, a method chosen for the high material density of the final layers, and the high damage thresholds that were reported in few experiments performed at other wavelengths and pulse durations [11, 15].

2.2. Test chamber

The test chamber is represented in figure 2. It is designed to match the peculiarities of the laser crystals geometry and mounting, ie circular disks intended to be dynamically rotated in the laser amplifier head in order to distribute the heat deposition over a large ring-shaped surface [9, 10]. The disks are therefore constrained by a central axis; the latter is used to maintain the disk over a water tub, with fused silica entrance and exit optical windows. The interval between the window glass and the crystal is set at the same range as in the laser head, namely, 1 mm. With this setup, two test beam paths are available, one for underwater experiments, and one for in-air experiments. The crystal can be easily rotated manually to exploit new crystal areas; the configuration restricts the areas that can be tested to those for which laser amplification is expected.

In a first set of experiments, the optical windows benefited from anti-reflection coatings. It turned out however that the latter presented lower laser damage thresholds (approximately 15 J/cm^2) than the laser crystals, thus impairing the measurement of the crystal damage threshold under water. In a long term laser amplification objective, the window anti-reflection coatings will have to be optimized in turn to reach higher damage thresholds; however, for the sake of this LIDT study on Yb:YAG disks, the issue was simply solved by resorting to uncoated fused silica windows, that exhibit damage thresholds at much higher values than any tested crystal configuration. The transmission of the uncoated windows in the experimental configuration was measured to be 93.5 %, consistent with the sum of the Fresnel reflectivities of the air/glass and glass/water interfaces. In the experimental handling of data, the laser pulse energy interacting with the crystal under water was then deduced from the externally measured and calibrated pulse energy by a 3.25% reduction.

2.3. Laser damage setup and characterization

The laser damage data were obtained on the BLANCO laser damage testbed, sketched in Figure 3 which has been previously described in details in ref. [16]. The BLANCO testbed is routinely used in the framework of the

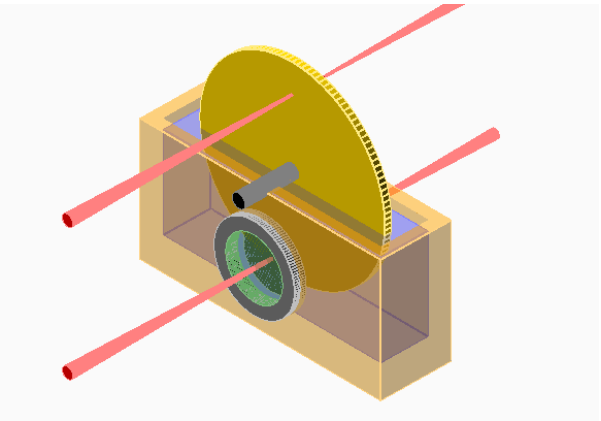

Figure 2: Sketch of the crystal test tub, with optical path (red) for in-air damage (above) and in-water damage (below).

Laser MegaJoule project, and has achieved a high reliability in laser damage threshold characterization [17, 18].

The setup is based on a Q-switched Nd:YAG laser operating at the 1064 nm fundamental wavelength. The laser delivers approximately 800 mJ at a nominal repetition rate of 10Hz, and may also shoot on a shot-on-demand basis for 1-on-1 studies. The laser beam is p-polarized, displays an almost top-hat profile with an entrance full width at half-maximum of 8mm, and is focused onto the sample by a convex lens whose focal length is $f = 4000$ mm. It induces a depth of focus (DOF) higher than the thickness of the test chamber (Fig. 2), ensuring the beam shape to be constant along the DOF, meaning that the shape and the diameter of the laser beam were the same on the front and on the rear surfaces of the crystal.

The test laser wavelength of 1064 nm differs little from the operating wavelength, 1030 nm. This slight wavelength difference is assumed not to play any significant role. Indeed, the spectral bandwidth of the anti-reflection coating extends over 200 nm, and beyond the longer wavelength; secondly, the dependence on laser wavelength of damage processes starts to be significant for much larger spectral differences, for instance between infrared and visible wavelengths, as was shown by Gallais et al. [19], Duchateau et al. [20] and Chambonneau et al. [21].

Due to the overall thickness of the test chamber, the main challenges to carry on damage tests were to avoid Kerr and Brillouin nonlinear processes.

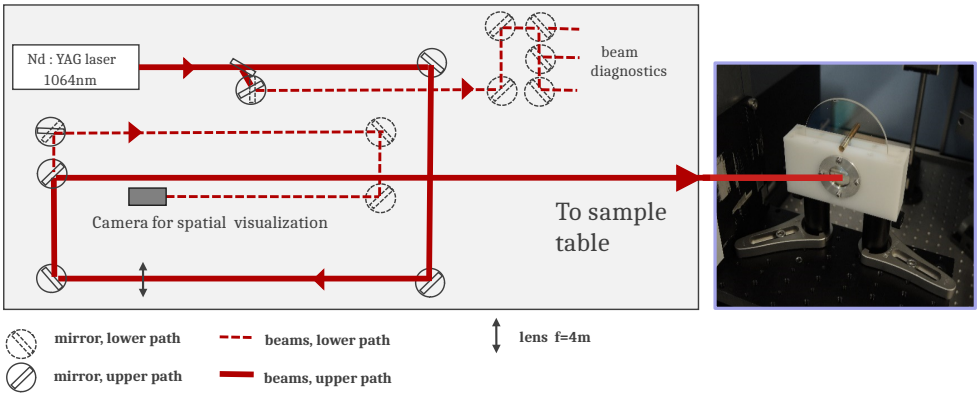

Figure 3: Layout of the optical system. Two beam paths are defined, the upper one for the LIDT measurement, the lower one for real time beam characterization. Upper right beam diagnostics : temporal and spectral controls.

Non-linear Kerr propagation could indeed lead to the formation of filaments resulting in unavoidable bulk damage. Brillouin non-linear propagation could lead to the initiation of front surface damage due to back stimulated Brillouin scattering [22]. These difficulties were solved by controlling the spatial and temporal intensity profiles of the laser pulses. A phase-modulated injection seeder allows operating the nanosecond Nd:YAG Q-switched laser with pulses having both a large spectral bandwidth with respect to the Brillouin shift, and a smooth temporal profile [23]. Figure 4(a) displays the pulse profile, as captured by a fast photodiode. The pulse full width at half maximum was 6.4 ns; in the context of laser damage studies, it is however more relevant to supply the equivalent pulse duration, ie, the ratio between pulse energy and maximum intensity [14]. The equivalent pulse duration was $\simeq 6.5 \pm 0.15$ ns.

Thanks to this smooth temporal waveform, such pulses were shown to allow one to reduce the impact of the Kerr effect and, because of the wide spectral bandwidth, to suppress stimulated Brillouin scattering [23]. In the following experiments, these non-linear processes were hence fully mastered by use of the injection seeder.

At the focal point, the beam spot had a millimetric size, and was mostly Gaussian-shaped (Fig. 4(b)). From the image, we determine the beam equivalent area $S_{eq} = 5.10^{-3}$ cm^2 as the ratio between the integrated measured fluence to the peak fluence [14]. This corresponds to an equivalent diameter

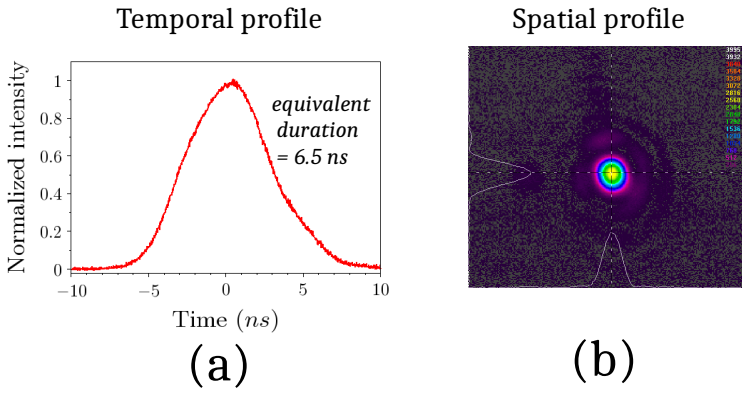

Figure 4: (a) Temporal profile of the injection-seeded laser, exhibiting an equivalent duration of 6.5 ± 0.15 ns. (b) Spatial profile of the focused laser beam. Image dimension of 6.8 mm.

of 800 ± 31 μm. This value can also be viewed as the beam diameter at $1/e$ in intensity for a pure Gaussian profile, in agreement with Fig. 4(b). Note i) that the measurement was performed on the diagnostics line at the image plane corresponding to the distance d between the focusing lens and the sample; and ii) that the beam diameter was actually measured on a shot-to-shot basis.

The energy measurements were also sampled on a shot-to-shot basis by a separate diagnostics line as shown in figure 3, and calibrated by a pyroelectric device. The standard deviation (σ) of shot-to-shot laser energy fluctuations was measured to be 0.9%. The relative full width at $\pm 2\sigma$ of the statistical distribution of fluences on target is estimated to less than 7%, the dominant source of uncertainty being the gradual drift in S_{eq} over time. This is the reason why the beam equivalent area was determined before each data acquisition. A conservative upper limit on fluence fluctuations can be considered at the level of 10% at 2σ [24].

2.4. Laser damage characterization procedures

Laser damage tests were conducted following the general procedure described by the ISO Standard [14], starting with 1-on-1 tests. About 20 sites were first tested per fluence, on the basis of an ensemble of about 10 fluence values. Any damage site of few tens of microns could be detected both on

the front face or at the rear face of the Yb:YAG crystal. The damage detection was performed thanks to a He-Ne laser beam propagating collinearly to the test beam. For each laser shot, we determine in real time if a damage site occurs or not, so as to extract a probability as function of fluence. Each occurrence was measured to make results independent from the laser fluctuations. The online detection was later ascertained by a post-mortem observation of detected damage sites using a Nomarski microscope, allowing us to validate unambiguously any damage occurrence. This first set of 1-on-1 experiments allowed the determination of the Laser-Induced Damage Thresholds (LIDT) of the crystal. These results are presented in paragraph 3.1. Rasterscan experiments [25] were then performed at fluences lower or close to the damage thresholds previously observed, to get additional information in conditions where the damage probability is small. Results are presented in paragraph 3.2.

3. Experimental results

3.1. 1-on-1 data

We present in figure 5 the damage probabilities obtained in the air and underwater environments from the standard 1-on-1 procedure, for sample A (5(a)) and sample B (5(b)).

The raw data were first treated by the cumulative procedure proposed by Jensen et al. [26], before the determination of the LIDT. The numerical value of the latter is often calculated by the method advised by the ISO standard [14], that is, as the fluence value for which the linear interpolation of damage probabilities between 0 and 1 reaches 0. This method was not applicable in our case with sufficient rigor, as the highest fluences achievable turn out not to be sufficient to saturate the damage processes. We therefore chose another procedure, in which the data are fitted by the Porteus and Seitel theoretical model for a power-law distribution of defects, taken in the Gaussian beam case [27], following the equation :

$$P(F) = 0 \qquad \text{for} \qquad F < F_{th} \tag{1}$$

$$= 1 - \exp\left[\frac{\pi w^2 N_p(F)}{(F/F_{th})^{p+1}} \int_1^{F/F_{th}} u^{-1}(u-1)^{p+1} du\right], \qquad \text{for} \qquad F > F_{th} \tag{2}$$

where $P(F)$ is the damage probability P at fluence F, F_{th} is the damage threshold fluence, w is the Gaussian beam waist at the interaction plane, $N_p(F)$ is the integral of the distribution function assuming a power law distribution of defects of index p [27].

The best fits are obtained by a least square optimization, based on the $\chi(2)$ of the data points with respect to the prediction of Eq. (2), and assuming constant uncertainties for all data points.

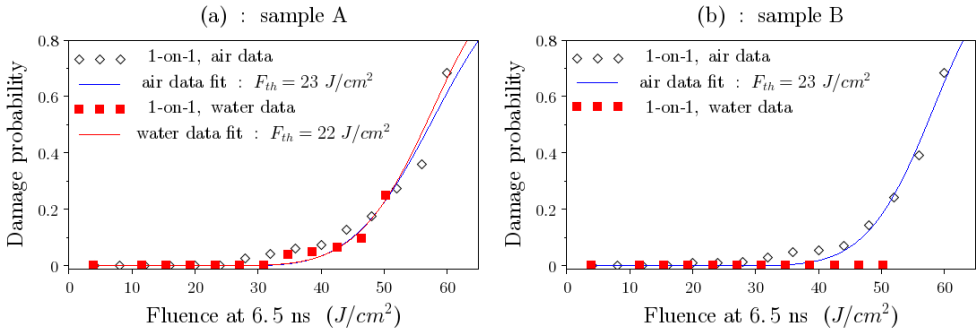

Figure 5: 1-on-1 experimental data obtained for the A and B samples (a and b respectively) in the air and underwater configurations, together with optimal model fits. Data handling makes use of the cumulative procedure of Jensen et al. [26] ; fits are based on the model of Porteus and Seitel [27].

For the A sample, the damage thresholds thus obtained are slightly higher than 20 J/cm^2, a value which is considered as nominal by the crystal manufacturer for HfO_2/SiO_2 IBS layers [28]; the values in air and underwater are similar. This is already very good news, as it validates the use of HfO_2/SiO_2 anti-reflection coatings on Yb:YAG slabs underwater in the same fluence conditions as in air.

The B sample actually exhibits a higher resistance to damage underwater than in air. The air result is again consistent with 20 J/cm^2; however, in a water environment, the B sample did not exhibit any damage in the whole series of tests, up to damage fluences of 50 J/cm^2. While it is not possible to perform a fit in such conditions, it appears extremely likely that the damage threshold for this sample is at least as high as 40 J/cm^2, a factor of 2 higher than in air. This will be discussed in sections 4 and 5.

3.2. Rasterscan data

Rasterscans are used to examine in more detail the fluence range close to the threshold fluence determined by 1-on-1 tests. In such experiments [14], a large number of sites are scanned in successive lines, with a single shot per site, allowing one to have access to small damage probabilities.

Tables 1 and 2 present the results of the rasterscan tests on both A and B samples, in air and under water respectively. Test areas of 1 cm^2 were defined, allowing for scans of 1100 shots per fluence and configuration; all areas were inspected *post mortem* to check that no damage was large enough to falsely classify a neighboring site as damaged.

The rasterscan data for the A sample in air are consistent with the result of the 1-on-1 data fit, with a threshold around 20 J/cm^2. The rasterscan under water indicates a value somehow higher, presumably close to 28 J/cm^2, while the 1-on-1 fit indicated a LIDT of 22 J/cm^2.

During the rasterscan on the B disk immersed under water, no damage at all was observed, up to a fluence of 28 J/cm^2, showing that the damage threshold is higher than this value, which is in agreement with the results from the 1-on-1 experiments, that show an LIDT of at least 40 J/cm^2.

All the data for both samples and in both environments turn out to be fully consistent between 1-on-1 and rasterscan measurements.

Fluence (J/cm^2)	12	20	24	28
A sample	0/1105	0/1105	19/1104	20/1106
B sample	0/1103	0/1109	4/1108	9/1112

Table 1: Rasterscan data in air : number of damage sites with respect to number of tested sites.

Fluence (J/cm^2)	20	28
A sample	0/1102	2/1102
B sample	–	0/1107

Table 2: Rasterscan data underwater : number of damage sites with respect to number of tested sites.

3.3. Damage location and Post-Mortem images

The location and morphology of some defects damage sites in air and under water may differ. Figure 6 shows microscope pictures of damage sites obtained in air (a, c and d) and underwater (b), ranked by increasing values of the fluence at which damage was observed.

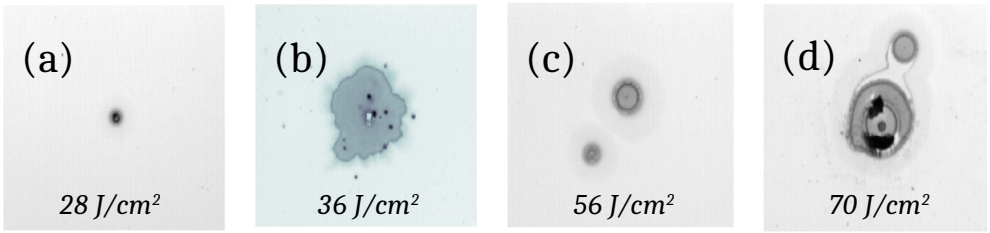

Figure 6: Post-mortem pictures of laser damage areas, for increasing laser fluences, in air and underwater. (a) in air at 28 J/cm^2; (b) underwater at 36 J/cm^2; (c) in air at 56 J/cm^2 ; and (d) in air at 70 J/cm^2. For an illustration purpose, the background color is chosen as grey in air, and blue for the underwater case. Each image has a dimension of 0.8 X 0.8 mm.

In air, the damage sites appear at the rear interface at the lowest fluences. At the highest fluences, we could notice also few damage sites at the entrance interface, mostly joint damage sites at the entrance and rear surfaces. Typical damage morphology is round, with sizes of the order of few tens of μm, except at extremely high fluences.

In contrast, defects obtained underwater were observed exclusively at the rear interface of the crystal. Their size could be much larger, in the 300 μm range, with irregular shapes, and faint dark lines on the periphery seeming to originate from a central point.

The fact that most damage sites are located at the rear surface is a known phenomenon, discussed by Papernov and Schmid [29]. Indeed, when a small scale damage starts, the absorption front results in a sharp bulk/plasma interface, that may either enhance or mitigate further laser absorption, depending on the relative position of the bulk and plasma at the rear or at the front respectively. This feature is therefore not distinctive of our experiment; we can note however that it draws our attention to the electromagnetic issues in the overall damage process.

4. Discussion

4.1. Discussion on experimental data

The first aim of the experiments was to compare the LIDT with the amplification saturation fluence of Yb:YAG, while keeping in mind the duration of our pulse, namely, 1 ns. However, all experimental data were obtained with a pulse duration of 6.5 ns; if we assume the $\sqrt{t}$ law [30], known to be strictly valid for glasses but also usually true for other optical materials , then the equivalent damage threshold at 1 ns can be obtained by dividing by $\sqrt{6.5} \simeq 2.5$. As a result, the damage threshold measured at 20 J/cm^2 both in air, or under water for sample A at 6.5 ns, translates into a 8 J/cm^2 threshold at 1 ns, which coincides with the saturation fluence of the Yb:YAG as measured by [8]. This opens up the prospect of an efficient laser amplification.

Secondly, the two samples used exhibit different behaviors. While the A sample yields damage thresholds are consistent with with typical values obtained for IBS hafnium oxide coatings in air, the B sample consistently gave null damage results underwater, pointing to a damage threshold as high as 40 J/cm^2 at 6.5 ns from the 1-on-1 data. It should be stressed that the 1-on-1 and rasterscan data are fully consistent in showing a major improvement in underwater conditions with respect to air conditions for the B sample; the results are also consistent for the A sample, with rasterscan data even pointing to a slightly higher LIDT underwater.

Thirdly, the morphology of the damage could be different in air and under water. The damage craters in air are standard; some damaged areas under water display irregular shapes over a large size.

These experimental findings may turn out to be of major importance for new generations of water face-cooled laser amplifiers at very high average power levels. Their origin should hence be investigated. The second and third points may hint that a specific microspic process is at stake, that may depend on the sample. However, more simple hypotheses should first be put under scrutiny : is it possible that temperature increases would appear on a slow time scale, differing between the two samples and between water or environments? Or could the different sample behaviors be due to their different thicknesses in view of non linear optical effects? We first consider these two hypotheses.

4.2. Discussion on potential thermal and non-linear optical effects

Let us first consider the thermal behavior of samples A and B under irradiation by the BLANCO laser. Temperature rises in the slabs, and in water may indeed be expected, due to linear laser absorption, and can be readily evaluated with elementary thermodynamics. The calculation differs for samples A and B, because of their different lengths, doping levels and volumes, also resulting in different optical paths in water, and different volumes of water in the tub.

The absorption coefficient of 1064 nm laser light in water is given by ref. [31] as 0.13 cm^{-1}. The beam paths in water were 1.8 mm and 2.7 mm for samples A and B, and the corresponding heat capacities of water in the tub were 60 and 67 J/K. Considering the setup to be thermalized, due to the low repetition rate at which the experiment was performed, this results in temperature rises in water of 6 mK and 8 mK for a series of 20 shots; of 0.3 K and 0.4 K for a rasterscan series of 1000 shots, again for samples A and B respectively.

Calculations of temperature rises by laser absorption within the slabs are similar. We take an upper limit to the Ytterbium ion absorption cross-section in the YAG crystal from the work of Brown et al. [32] ; and heat capacities given by the crystal manufacturer. Yb:YAG happens to be essentially transparent to 1064 nm light at room temperature. This results in extremely low temperature rises of only 0.002 K for 20 shots, for both samples, or less than 0.1K for 1000 shots. We note that the temperature rises for samples A and B are actually similar, as volume, length and doping effects tend to compensate one another.

These remain very low figures; in comparison, the detailed theoretical and experimental study by K. Mikami et al. [33] shows that it takes temperatures variations of the order of 100K to start seeing some changes in Laser-Induced Damage Thresholds.

From these thermodynamic calculations, we conclude that macroscopic thermal effects are highly unlikely to be the origin of the difference in behaviors between the two samples, and of the improved LIDT for sample B underwater.

Apart from thermodynamic phenomena, optical and especially non-linear optical processes might depend on the sample doping levels and thicknesses.

We do not expect any effect of doping – the doping levels were 1.5 and 2 atom-%, which are low numbers, that do not affect the lattice structure.

Doping affects the thermal conductivity, but a 0.5 % difference in doping levels is a negligible level.

Non-linear optical effects might occur differently, due to the 1-mm length difference between the samples. Two spurious non-linear processes could in principle depend on the sample length : Brillouin and Kerr.

As explained in section 2.3, the BLANCO test facility operates in a large spectral bandwidth mode, designed to mitigate the Brillouin instability [23]. A test was performed in the course of the experiment, by reverting briefly to a narrow bandwidth operation; whether in large or narrow bandwidth mode, no effect of Brillouin backscattering was detected.

A Kerr self-focusing effect could also depend on the sample length. In a separate experiment, this process was experimentally investigated on the BLANCO facility. The result is that Kerr-induced self-focusing is negligible for all samples less than 10 mm in length – which is largely the case here. Therefore, the difference in LIDT behaviors can not be due to the slightly different thicknesses between these two thin samples.

5. Electromagnetic model with lacunar permeation

Once *macroscopic* thermal or non-linear optical effects are ruled out as the origin of the experimental observations, we may explore how *microscopic* effects may come into play, in the process of laser-induced damage underwater.

The admitted general scenario for laser induced damage is as follows [34]. During the first stage, the laser pulse is absorbed through intrinsic processes or defects. In the case of intrinsic processes, absorption is due to nonlinear electronic processes including multiphoton absorption. In the case of precursor defects, the material band structure is modified locally, possibly leading to linear absorption. For both cases, the complex refractive index is modified prior to or during the interaction. For nanosecond laser pulses with moderate intensities, the scenario based on defects is the most probable [34, 35, 36]. During the second stage, the local material temperature rises due to absorption, leading to an increase in the pressure and possibly the formation of a shock wave. The latter may then induce structural defects, leading to the observed damage.

At first glance, the presence of water is expected to increase the plasma pressure through a confinement effect (as for laser produced shock waves

for various applications [37, 38]), and thus increase the damage probability, resulting in a decrease in the laser damage threshold. Since the opposite behavior is observed, this suggests an influence of water different from the contribution to the hydrodynamic response. The first stage of damage process relies on both the local value of the laser intensity and complex refractive index. Since the refractive index of water is 1.33, which is significantly different from unity (air), we suggest that it is the laser propagation and local laser intensity variations that can be influenced by water.

Pu et al. already observed improvements of LIDTs when the highly reflective coatings they studied had a water layer due to ambiant moisture in air, with respect to the vacuum conditions in which any water is removed [13]. However, their model, based on the asymmetric changes in thermal conductivity in air and vacuum, does not look adequate to our conditions. The experimental conditions for which they observed the highest LIDTs actually correspond to those for which we measure the lowest LIDTs. The physical regime is therefore clearly different.

We therefore present here a model that concentrates on the electromagnetic issues of wave propagation in a layered medium, taking into account the existence of damage precursors, namely micro-defects close to the surface of the YAG crystal.

Two types of micro-defects are known to exist : metallic nanoparticles as residues of the polishing powders; or nanometric or micrometric voids, for instance cracks resulting from subsurface damage [39] (SSD) created during grinding and polishing of the YAG crystal. We consider in particular the possibility of nanometric voids at the interface between YAG and the multilayer coating, which might be planar in case of stress-induced grazing between crystal and layers, or appearing as ribbons in case of mechanical scratches. The role of these sub-surface damage and defect precursors has been understood as instrumental to trigger high flux optical damage [39]; our approach follows directly from the discussion of Grua et al. [40] on surface scratches. We bring forward the hypothesis that, when the sample is brought into the cooling water, such voids may be gradually filled with the coolant, on the timescale of several hours or days, as the air gets dissolved through the layer porosity. Fluid permeation into a porous media is a known subject in other fields of physics [41]. Physics of permeation is of high complexity, as the resulting permeability depends not only on the layer porosity [42], but also on shape factors during the deposition process, and on such by-processes as oxidation and carbonization. From Darcy's law [41], and considering the

typical thicknesses of multilayers, size of micro-voids, centimetric immersion depths, and water kinematic viscosity, it turns out that permeabilities as low as 10^{-26} m^2 would be sufficient to fill in internal lacuna with water over few tens of hours. Therefore, it appears fully possible that a slow water permeation process may occur in immersed optical coatings, sufficient to fill in the internal lacuna with water, or with any other small molecule outer medium. In this water permeation scenario, the optical index within the voids matches that of the external environment, whether air or water. A one dimensional electromagnetic model is sufficient to capture the essential physical elements.

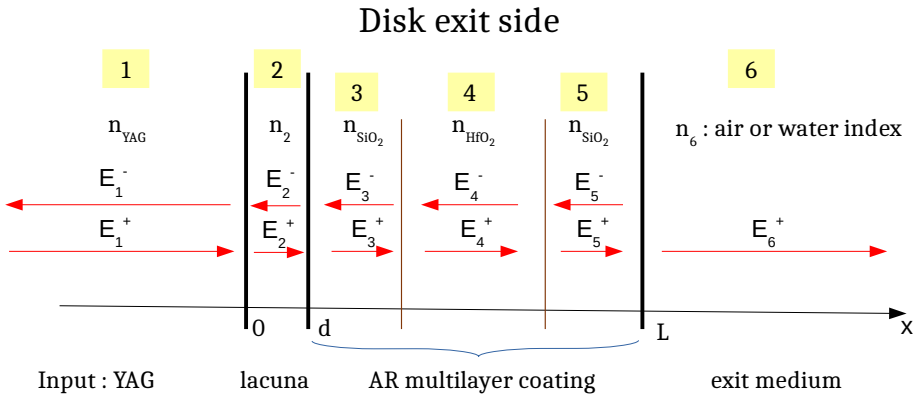

Figure 7: Scheme of the 1D electromagnetic model, in which the rear surface of the YAG crystal (area 1) presents a lacuna, ie a microscopic void volume (area 2) due for instance to a scratch, sandwiched between the garnet and the antireflection multilayer, that makes the transition to the outer medium (area 6). In the lacuna permeation hypothesis, the optical index of the micro-void matches that of the exit medium.

The model structure of the rear surface is represented in figure 7, with 4 sections : first the Yb:YAG bulk volume (area 1), then the lacuna (area 2), whose width may range typically from few nanometers to tens of nanometers; then the anti-reflection coating, composed of 3 layers (areas 3, 4 and 5); and finally the exit medium (area 6), which may be either air or water. The anti-reflection coating is taken in a common three-layer configuration [43], with a theoretical reflection ratio less than 10^{-4}.

Modeling the wave propagation in this 1D model is similar to the general modeling of any multi-layer structure. The electric fields are noted as $E_i^{\pm}(z)$, where the i stands for the area number; the exponent indicates whether the

wave is along the incident direction (label +, left to right propagation on the figure) or along the reflection direction (label −). Each amplitude $E_i^{\pm}$ is taken at the right frontier of the area, except for the exit medium, where it is taken at the left frontier.

For each intermediate layer, the transition and electromagnetic equations can be put in matrix form [44]:

$$\begin{pmatrix} E_{i-1}^{+} \\ E_{i-1}^{-} \end{pmatrix} = U_i \begin{pmatrix} E_i^{+} \\ E_i^{-} \end{pmatrix} \quad \text{with} \quad U_i = \frac{1}{2n_{i-1}} \begin{pmatrix} (n_{i-1}+n_i)e^{j\varphi_i} & (n_{i-1}-n_i)e^{-j\varphi_i} \\ (n_{i-1}-n_i)e^{j\varphi_i} & (n_{i-1}+n_i)e^{-j\varphi_i} \end{pmatrix}, \tag{3}$$

with $\varphi_i = n_i k_0 dx_i$, $i = 2$ to 5, where k_0 is the vacuum wavevector at the laser frequency, dx_i is the physical length of area i, and $\varphi_6 = 0$.

Matrix multiplication yields for the whole structure :

$$\begin{pmatrix} E_1^{+} \\ E_1^{-} \end{pmatrix} = U \begin{pmatrix} E_6^{+} \\ 0 \end{pmatrix} \quad \text{with} \quad U = U_2\ U_3\ U_4\ U_5\ U_6 = \begin{pmatrix} u_{11} & u_{12} \\ u_{21} & u_{22} \end{pmatrix},$$

from which the overall reflected field E_1^- and transmitted field E_6^+ can be deduced as :

$$E_6^+ = \frac{1}{u_{11}} E_1^+$$
$$E_1^- = \frac{u_{21}}{u_{11}} E_1^+.$$

Calculation of field values within each area is then straightforward.

Based on this numerical approach, figure 8 presents the total intensity $n|E^+(z) + E^-(z)|^2$ relative to the incident intensity, along the structure, in three cases : air permeation, with air void in area 2 and air output in area 6 ($n_2 = n_6 = 1$: blue line); water permeation, with water-filled void in area 2 and water output in area 6 ($n_2 = n_6 = 1.33$: red line) ; and a no permeation scenario, with air void in area 2 and water output in area 6 ($n_2 = 1$, $n_6 = 1.33$: black line). Fields are computed in the case of a 80-nm thick lacuna.

The existence of the defect breaks the optimal negative interference process between reflected waves in the layers, that makes the coating anti-reflecting in normal conditions. The spurious reflection induced by the defect leads to interferences both in the YAG and in the multi-layers; however, figure 8 shows that this interference effect is more severe on the YAG side, which happens to be the area with the largest density of defects [45]. These

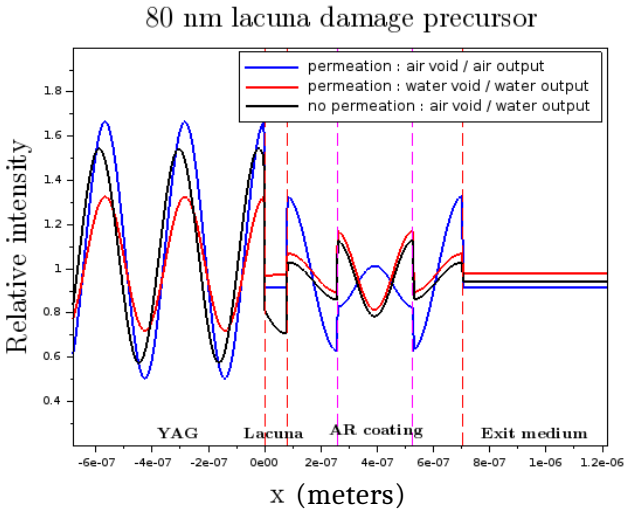

Figure 8: Laser relative intensity distributions in the successive areas, showing the intensity enhancements in the YAG bulk close to the surface, in the permeation scenarios (water/water, air/air), and in a no-permeation scenario (air void /water output) . The nominal exit intensity is taken as the reference.

interferences result in local over intensities, that are directly responsible for damage initiation and enhancement.

The water/water situation, corresponding to the case where water has permeated through the layer porosity to fill the lacuna, presents the smallest value of over intensities; conversely, the air/air situation presents the highest over intensities.

Non permeation of water would lead to lacuna remaining full of air even when the slab is immersed under water. This situation, shown in black, exhibits intermediate excess intensity values, and should therefore induce more damage events than in the water permeation case.

This is possibly the origin of the different behaviors observed between samples A and B, as the permeation is known to be a slow process, and the time of previous immersion of each sample may have differed.

6. Conclusion

This article reports experimental results concerning the laser-induced damage threshold of Yb:YAG laser crystals with an Ion Beam Sputtering

Hafnium oxide - Silicon oxide anti-reflection coating, and operated underwater for direct face cooling. With no previous reported result of that type, the possibility that the damage thresholds would be worse underwater than in air was initially considered as a serious technical risk. On the contrary, our experimental results indicate that laser crystals coated by IBS HfO_2/SiO_2 multilayers may operate underwater with damage thresholds at least as high as in air, with one sample exhibiting major resistance to laser damage.

A one-dimensional electromagnetic model, based on the permeation of water into the precursor lacuna was proposed, that gives predictions qualitatively consistent with the observations. Obtaining any quantitative agreement is obviously not the objective – a one dimensional electromagnetic model is not fit for that, as it would require three-dimensional modeling of a realistic surface defect such as a microscopic scratch. However, one dimensional models are known to supply physically relevant considerations on field amplitudes, and have been extensively used for that [46]. We therefore put forward the hypothesis that this lacuna permeation scenario might be one possible explanation to the different behaviors observed between samples A and B, as the permeation status of the samples was not known. Other studies will be required, either to propose alternative or complementary explanations, or to explore the physics of fluid permeation into optical coatings.

In summary, our results show that the resilience to laser damage may be at least as high underwater as in air. In the case of Yb:YAG slabs amplifier immersed in water, the fluence of laser damage threshold is higher than or equal to the saturation fluence of Yb:YAG for a 1-ns pulse duration. From a laser development perspective, especially for chirped pulse amplification technologies based on Ytterbium:YAG media, this is important to compare the advantages and drawbacks of the different solid-state, diode-pumped, high average power amplification technologies. Helium face-cooling at cryogenic temperatures allows indeed for enhanced amplification cross-sections of Ytterbium:YAG, on a reduced amplification bandwidth; conversely, liquid face-cooling at positive temperatures allows for amplification on a broader bandwidth, consistent with one-picosecond amplified pulses, at the expense of a higher saturation fluence of 8 J/cm^2. This work shows that the underwater laser-induced damage thresholds can reach indeed this value for 1 nanosecond amplified pulses. This is an essential piece of information for all laser development projects, similar to the HORIZON project [10], based on direct face-cooling of immersed amplifier slabs, and aiming to address the need for future MegaJoule-class, high repetition rate lasers as drivers for

Inertial Confinement Fusion facilities.

The present study should be viewed as a preliminary exploration of the underwater damage behaviors and mechanisms. Further investigation and systematic exploration of materials, conditions, and permeation regime are required; our study thus opens exciting new perspectives to study the detailed mechanisms of laser damage in a liquid environment.

Acknowledgments

This work is part of the LEAP project, supported by Région Aquitaine (contract 16005645), European Structural Funds (contract 2779610), Université de Bordeaux, CEA and CNRS. Multilayer coatings from Advanced Thin Films, Boulder, Colorado, USA are acknowledged.

References

[1] H. Okada, H. Yoshida, H. Fujita, M. Nakatsuka, Liquid-cooled ceramic Nd:YAG split-disk amplifier for high-average-power laser, Opt. Commun. 24 (2006) 816.

[2] J. Zuegel, M. Shoup, J. Kelly, C. Frederickson, Novel actively cooled split-disk Nd:glass laser amplifier for high-energy applications with improved repetition rate, in: Advanced Solid-State Photonics, Optical Society of America, 2011, p. ATuB1.

[3] A. Giesen, J. Speiser, Fifteen years of work on thin-disk lasers: results and scaling laws, IEEE J. Sel. Top. Quant. Elec. 13 (2007) 598.

[4] M. Divoký, J. Pilař, M. Hanuš, P. Navrátil, O. Denk, P. Severová, P. Mason, T. Butcher, S. Banerjee, M. De Vido, C. Edwards, J. Collier, M. Smrž, T. Mocek, 150 J DPSSL operating at 1.5 kW level, Optics Letters 46 (2021) 5771. doi:10.1364/OL.444902.

[5] R. Chonion, J. M. Sajer, E. Bordenave, F. Le Palud, P. M. Dalbies, J. Néauport, Multiphysics model of liquid-cooled Nd:phosphate split-slabs in large aperture optical amplifiers, Opt. Express 28 (2020) 20162–20176.

[6] K. Wang, B. Tu, C. Jia, J. Shang, X. An, Y. Liao, Z. Xu, J. Guo, J. Yi, Y. Yu, 7 kW direct-liquid-cooled side-pumped Nd:YAG multi-disk laser resonator, Opt. Express 24 (2016) 15012–15020.

[7] H. Wang, A. R. Meadows, E. Jankowska, E. Randel, B. A. Reagan, J. J. Rocca, C. S. Menoni, Laser Induced Damage in coatings for cryogenic Yb:YAG active mirror amplifiers, Opt. Lett. 45 (2020) 4476–4479. doi:10.1364/OL.399293.

[8] X. Yan, J. Zheng, X. Jiang, M. Li, M. Li, Z. Wang, Gain saturation study and measurement of terminal level lifetime for Yb: YAG crystal, Laser Physics Letters 11 (2014) 125002.

[9] S. Petit, Ch. Féral, M.-Ch. Nadeau, Ph. Balcou, J. Brandam, D. Descamps, J. Lhermite, D. Marion, Towards a kW-class picosecond laser at 1 kHz, in: O. T. Digest (Ed.), 2019 Conference on Lasers and Electro-Optics Europe and European Quantum Electronics Conference, Optica Publishing Group, 2019.

[10] J. Lhermite, Ch. Féral, D. Marion, A. Rohm, Ph. Balcou, D. Descamps, S. Petit, M.-Ch. Nadeau, E. Mével, HORIZON laser: a new generation of kw-class ps amplifier, in: International Conference on Advanced Laser Technologies (ALT), 21, Prokhorov General Physics Institute of Russian Academics of Sciences, 2021, p. 133.

[11] M. Alvisi, M. Di Giulio, S. Marrone, M. Perrone, M. Protopapa, A. Valentini, L. Vasanelli, HfO_2 films with high laser damage threshold, Thin Solid Films 358 (2000) 250–258. doi:10.1016/S0040-6090(99)00690-2.

[12] D. N. Nguyen, L. A. Emmert, P. Schwoebel, D. Patel, C. S. Menoni, M. Shinn, W. Rudolph, Femtosecond pulse damage thresholds of dielectric coatings in vacuum, Optics Express 19 (2011) 5690–5697.

[13] Y. Pu, P. Ma, S. Chen, J. Zhu, G. Wang, F. Pan, P. Sun, X. Zhu, J. Zhu, D. Xiao, Mechanism for atmosphere dependence of laser damage morphology in HfO_2/SiO_2 high reflective films, Journal of Applied Physics 112 (2012) 023111. doi:10.1063/1.4737405.

[14] ISO Standard 11254-1, ISO Standard 11254-2, Lasers and laser-related equipment – test methods for laser-induced damage threshold, 2001.

[15] B. Langdon, D. Patel, E. Krous, J. J. Rocca, C. S. Menoni, F. Tomasel, S. Kholi, P. R. McCurdy, P. Langston, A. Ogloza, Influence of process conditions on the optical properties of HfO_2/SiO_2 coatings for high-power laser coatings, in: G. J. Exarhos, A. H. Guenther, K. L. Lewis, D. Ristau, M. J. Soileau, C. J. Stolz (Eds.), Laser-Induced Damage in Optical Materials: 2007, volume 6720, International Society for Optics and Photonics, SPIE, 2008, p. 67200X. doi:10.1117/12.753027.

[16] M. Chambonneau, M. Chanal, S. Reyné, G. Duchateau, J.-Y. Natoli, L. Lamaignère, Investigations on laser damage growth in fused silica with simultaneous wavelength irradiation, Applied Optics 54 (2015) 1463.

[17] S. Reyné, G. Duchateau, J. Natoli, Competition between ultraviolet and infrared nanosecond laser pulses during the optical breakdown of KH_2PO_4 crystals, Appl. Phys. B 09 (2012) 695–706. doi:10.1007/s00340-012-5238-8.

[18] S. Bouillet, C. Ameil, V. Beau, O. Bonville, S. Cavaro, R. Courchinoux, J. Daurios, T. Donval, L. Eupherte, S. Fréville, G. Gaborit, I. Lebeaux, C. Leymarie, S. Martin, R. Parreault, G. Razé, N. Roquin, L. Lamaignère, Large optics metrology for high-power lasers, J. Opt. Soc. Am. A 36 (2019) C95–C103. doi:10.1364/JOSAA.36.000C95.

[19] L. Gallais, D.-B. Douti, M. Commandre, G. Bataviciute, E. Pupka, M. Sciuka, L. Smalakys, V. Sirutkaitis, A. Melninkaitis, Wavelength dependence of femtosecond laser-induced damage threshold of optical materials, J. App. Phys. 117 (2015) 223103.

[20] G. Duchateau, M. D. Feit, S. G. Demos, Transient material properties during defect-assisted laser breakdown in deuterated potassium dihydrogen phosphate crystals, J. App. Phys. 115 (2014) 103506. doi:10.1063/1.4868161.

[21] M. Chambonneau, J.-L. Rullier, P. Grua, L. Lamaignère, Wavelength dependence of femtosecond laser-induced damage threshold of optical materials, Opt. Express 26 (2018) 21819.

[22] L. Lamaignère, K. Gaudfrin, T. Donval, J. Natoli, J. Sajer, D. Penninckx, R. Courchinoux, R. Diaz, Laser-induced damage of fused silica

optics at 355 nm due to backward stimulated Brillouin scattering: experimental and theoretical results, Optics Express 26 (2018) 11744–11755.

[23] D. Penninckx, J. Luce, R. Diaz, O. Bonville, R. Courchinoux, L. Lamaignère, Multiple-frequency injection-seeded nanosecond pulsed laser without parasitic intensity modulation, Optics Lett. 41 (2016) 3237.

[24] S. Bouillet, C. Ameil, V. Beau, O. Bonville, S. Cavaro, R. Courchinoux, J. Daurios, T. Donval, L. Eupherte, S. Freville, G. Gaborit, I. Lebeaux, C. Leymarie, S. Martin, R. Parreault, G. Raze, N. Roquin, , L. Lamaignère, Large optics metrology for high-power laser, Journal of the Optical Society of America A 36 (2019) C95.

[25] L. Lamaignère, S. Bouillet, R. Courchinoux, T. Donval, M. Josse, J.-C. Poncetta, H. Bercegol, An accurate, repeatable, and well characterized measurement of laser damage density of optical materials, Review of Scientific Instruments 78 (2007) 103105. URL: http://aip.scitation.org/doi/10.1063/1.2796148. doi:10.1063/1.2796148.

[26] L. Jensen, M. Mrohs, M. Gyamfi, H. Mädebach, D. Ristau, Higher certainty of the laser-induced damage threshold test with a redistributing data treatment, Review of Scientific Instruments 86 (2015) 103106. URL: http://aip.scitation.org/doi/10.1063/1.4932617. doi:10.1063/1.4932617.

[27] J. O. Porteus, S. C. Seitel, Absolute onset of optical surface damage using distributed defect ensembles, Applied Optics 23 (1984) 3796. doi:10.1364/AO.23.003796.

[28] Z. Cole, Teledyne FLIR laser crystals sample LDT data bank (2022) private communication.

[29] S. Papernov, A. W. Schmid, Testing asymmetry in plasma-ball growth seeded by a nanoscale absorbing defect embedded in a SiO2 thin-film matrix subjected to uv pulsed-laser radiation, J. Appl. Phys. 104 (2008) 063101.

[30] B. C. Stuart, M. D. Feit, A. M. Rubenchik, B. W. Shore, M. D. Perry, Laser-Induced Damage in dielectrics with nanosecond to subpicosecond pulses, Physical Review Letters 74 (1995) 2248–2251. doi:10.1103/PhysRevLett.74.2248.

[31] V. V. Semak, A. Gerakis, M. N. Shneider, Measurement of temperature dependent absorption coefficient of water at 1064 nm wavelength, AIP Advances 9 (2019) 085016. doi:10.1063/1.5085746.

[32] D. C. Brown, R. L. Cone, Y. Sun, R. W. Equall, Yb:YAG absorption at ambient and cryogenic temperatures, IEEE J. Sel. Top. QE 11 (2005) 604. doi:10.1109/JSTQE.2005.850236.

[33] K. Mikami, S. Motokoshi, T. Somekawa, T. Jitsuno, M. Fujita, K. Tanaka, H. Azechi, Theoretical analysis for temperature dependence of laser- induced damage threshold of optical thin films, J. Phys.: Conf. Series 688 (2016) 012065. doi:10.1088/1742-6596/688/1/012065.

[34] R. M. Wood, Laser-Induced Damage of Optical Materials, CRC Press, Boca Raton, 2003.

[35] G. Duchateau, M. Feit, S. Demos, Strong nonlinear growth of energy coupling during laser irradiation of transparent dielectrics and its significance for Laser Induced Damage, Journal of Applied Physics 111 (2012) 093106. doi:10.1063/1.4707755.

[36] D. Ristau, Laser-Induced Damage in Optical Materials, CRC Press, Boca Raton, 2015.

[37] L. Berthe, R. Fabbro, P. Peyre, E. Bartnicki, Wavelength dependent of laser shock-wave generation in the water-confinement regime, Journal of Applied Physics 85 (1999) 7552. doi:10.1063/1.370553.

[38] L. Berthe, R. Fabbro, P. Peyre, L. Tollier, E. Bartnicki, Shock waves from a water-confined laser-generated plasma, Journal of Applied Physics 82 (1997) 2826. doi:10.1063/1.366113.

[39] T. Suratwala, L. Wong, P. Miller, M. Feit, J. Menapace, R. Steele, P. Davis, D. Walmer, Sub-surface mechanical damage distributions during grinding of fused silica, Journal of Non-Crystalline Solids 352 (2006) 5601–5617. doi:10.1016/j.jnoncrysol.2006.09.012.

[40] P. Grua, L. Lamaignère, M. Chambonneau, R. Courchinoux, J. Néauport, Nanosecond laser damage initiation at $0.35\mu m$ in fused silica, Opt. Lett. 43 (2018) 2692–2695. URL: http://opg.optica.org/ol/abstract.cfm?URI=ol-43-11-2692. doi:10.1364/OL.43.002692.

[41] K. Wittman-Ténèze, N. Caron, S. Alexandre, Gas permeability of porous plasma sprayed coatings, Journal of Thermal Spray Technology 17 (2008) 902. doi:10.1007/s11666-008-9262-5.

[42] B. Huang, W. Le, Y. Wang, X. Luo, Y. Yang, Microstructure, properties and thermal stability of W/B_4C multilayer coating synthesized by ion beam sputtering, Applied Surface Science 464 (2019) 10–20. doi:10.1016/j.apsusc.2018.09.077.

[43] O. S. Heavens, Optical properties of thin films, Rep. Prog. Phys 23 (1960) 1.

[44] M. A. Swillam, M. H. Bakr, X. Li, The design of multilayer optical coatings using convex optimization, J. Lightwave Tech. 4 (2007) 1078–1085. doi:10.1109/JLT.2007.891457.

[45] J. Néauport, L. Lamaignère, H. Bercegol, F. Pilon, J.-C. Birolleau, Polishing-induced contamination of fused silica optics and laser induced damage density at 351 nm, Optics Express 13 (2005) 10163. doi:10.1364/OPEX.13.010163.

[46] S. Papernov, A. A. Kozlov, J. B. Oliver, C. Smith, L. Jensen, S. Günster, H. Mädebach, D. Ristau, Role of HfO2/SiO2 thin-film interfaces in near-ultraviolet absorption and pulsed laser damage, Optical Engineering 56 (2017) 011004–011004. doi:10.1117/1.OE.56.1.011004.